

Article

Tribological Properties and Physiochemical Analysis of Polymer-Ceramic Composite Coatings for Bone Regeneration

Agnieszka Maria Tomala ^{1,*}, Dagmara Słota ¹, Wioletta Florkiewicz ¹, Karina Piętak ¹, Mateusz Dyląg ^{1,2} and Agnieszka Sobczak-Kupiec ¹

¹ Department of Materials Science, Faculty of Materials Engineering and Physics, Cracow University of Technology, 37 Jana Pawła II Av., 31-864 Cracow, Poland; dagmara.slota@doktorant.pk.edu.pl (D.S.); wioletta.florkiewicz@pk.edu.pl (W.F.); karina.pietak@doktorant.pk.edu.pl (K.P.); mateusz.dylag@atmat.pl (M.D.); agnieszka.sobczak-kupiec@pk.edu.pl (A.S.-K.)

² ATMAT Sp. z o.o., Siwka 17, 31-588 Cracow, Poland

* Correspondence: agnieszka.tomala@pk.edu.pl

Abstract: The biomaterial coatings for bone tissue regeneration described in this study promote bioactivity. The ceramic-polymer composite coatings deposited on polylactide (PLA) plates contain polymers, namely polyvinylpyrrolidone (PVP)/polyethylene glycol (PEG), while the ceramic phase is hydroxyapatite (HA). Additionally, collagen (COL) and glutathione (GSH) are components of high biological value. Bone tissue materials requires additionally demanding tribological properties, which are thoroughly described in this research. These findings, presented herein for the first time, characterize this type of highly specific composite coating material and their indicate possible application in bone regeneration implants. Implementation of the collagen in the PVP/PEG/HA composite matrix can tailor demanding tribological performance, e.g., anti-wear and friction reduction. The addition of the ceramic phase in too high a content (15%) leads to the decreased swelling ability of materials and slower liquid medium absorption by composite coatings, as well as strong surface roughening and loosening tribological properties. In consequence, small particles of HA from the very rough composite crumble, having a strong abrasive effect on the sample surface. In conclusion, sample C composed of PVP/PEG/GSH/COL/HA (5%) exhibits high bioactivity, strong mechanical and tribological properties, the highest free surface energy, porosity, and accepted roughness to be implemented as a material for bone regeneration.

Keywords: biomaterials; coatings; hydroxyapatite; tribology



Citation: Tomala, A.M.; Słota, D.; Florkiewicz, W.; Piętak, K.; Dyląg, M.; Sobczak-Kupiec, A. Tribological Properties and Physiochemical Analysis of Polymer-Ceramic Composite Coatings for Bone Regeneration. *Lubricants* **2022**, *10*, 58. <https://doi.org/10.3390/lubricants10040058>

Received: 2 March 2022

Accepted: 22 March 2022

Published: 2 April 2022

Publisher's Note: MDPI stays neutral with regard to jurisdictional claims in published maps and institutional affiliations.



Copyright: © 2022 by the authors. Licensee MDPI, Basel, Switzerland. This article is an open access article distributed under the terms and conditions of the Creative Commons Attribution (CC BY) license (<https://creativecommons.org/licenses/by/4.0/>).

1. Introduction

A significant feature of medical devices including implants that has been emphasized in recent years is their multifunctionality to ensure effective and long-lasting function. One solution that can provide this involves coating the implants, thereby creating specific films [1]. The coating technique requires a layer of another biomaterial to cover the surface of the implant [2]. Coating implants is one strategy used to increase biocompatibility as well as provide additional features without changing the based material. In the case of materials developed for bone regeneration, coating can be used to add the desired feature of improved osseointegration. Furthermore, coating implants with a layer can be very useful in increasing tissue cell adhesion to the surface and inhibiting bacterial colonization [3]. The most effective osseointegration-promoting properties can be achieved by coating the materials with bioactive calcium phosphate ceramics (CaP). The presence of a bioactive CaP coating can not only help to form a stable interface between the implant and the bone, but also block the diffusion of toxic elements from the implant into the body, especially when coating metallic components [4,5].

Osseointegration itself depends on the mechanical bonding between bone and implant after surgical placement as well as the cellular response at the bone-implant interface, hence the importance of proper material selection [6]. Therefore, among the CaP, hydroxyapatite (HA) is particularly interesting in the context of bone regeneration as it exhibits osteoconductive abilities that are important in this process [7]. A better connection between the implant and natural tissue eliminates the danger of implant loosening, which has contributed to the failure of biomaterial application in the patient's body over the past two decades [8]. Frequently, HA itself is used as a coating material by applying it to the implant surface by various techniques, including plasma spraying or laser surface treatment [9,10]. Of particular interest in this aspect is the ability to provide osteoconductive conditions through which surrounding tissues can bind to HA [11]. Additionally, it can be modified with Sr and Zn ions to impart antimicrobial properties or increase wettability [12]. However, it is still difficult to eliminate the basic application limitations of HA, which are brittleness and low mechanical strength. These properties limit its potential in terms of use for load-bearing implants [13]. The solution to this problem may be to suspend the HA in a polymer matrix, as this will give flexibility [14,15].

As polymeric biomaterials, polymers that are biologically safe and do not exhibit cytotoxicity or allergic reactions are used [16]. Polyvinylpyrrolidone (PVPP) is a water-soluble substance approved by the U.S. Food and Drug Administration (FDA) as non-toxic and safe for body contact [17,18]. It exhibits excellent physiological biocompatibility as well as good adhesion [19,20]. Another synthetic polymer that is also characterized by high solubility, biocompatibility, as well as good tolerance is poly(ethylene glycol) (PEG). It is non-immunogenic and for this reason is suitable for medical applications, including as a carrier for active substances [21,22]. Furthermore, the FDA has approved PEG-conjugated drugs for safe use in humans [23]. An otherwise equally interesting polymeric material being considered for bone tissue regeneration is polylactic acid (PLA). Due to its properties, such as biocompatibility, biodegradability, and osteoconductive ability, it is used as a material for drug delivery systems, surgical implants, as well as tissue growth films [24–27].

The presented work describes the results of research on innovative ceramic–polymer composite coatings containing glutathione and bioactive calcium phosphate for bone tissue regeneration. The objective of this study was to obtain a highly flexible and wear-resistant composite coating for implants. The materials have great potential considering the high biological value of the components used in their synthesis, such as glutathione and hydroxyapatite, which promote osteogenesis. So far, no other solution of this type has been found.

2. Materials and Methods

2.1. Reagents

The reagents used for the synthesis of HA, i.e., the sodium phosphate dibasic (Na_2HPO_4) (7558-79-4), calcium acetate monohydrate ($\text{Ca}(\text{CH}_3\text{CO}_2)_2 \cdot \text{H}_2\text{O}$) (5743-26-0), and ammonia water (NH_4OH , 25%) (1336-21-6), as well as polymers polyvinylpyrrolidone (PVP) (9003-39-8), polyethylene glycol (PEG) (25322-68-3), poly(ethylene glycol) Mn 575 diacrylate Mn 575 (PEGDA) (26570-48-9), 2-hydroxy-2-methylpropiophenone 97% (7473-98-5), peptide l-glutathione reduced 98% (GSH) (70-18-8), collagen from bovine achilles tendon (COL) (9007-34-5), and diiodomethane 99% (75-11-6) were obtained from Sigma-Aldrich (Darmstadt, Germany). Ultra-high quality (UHQ) water was purchased from Elga Purelab UHQ (Marlow, Buckinghamshire, UK).

2.2. Preparation of Coatings

A 15% PVP solution and a 15% PEG solution were prepared to obtain mixtures for the preparation of composites. Suitable amounts of the solutions so prepared and HA powder obtained as previously in [28] were used to obtain the blends used for the preparation of coatings. In the first step, 0.25 mL of PVP 15% mixture with GSH was applied to polylactide (PLA) plates with dimensions of 2 cm × 2 cm × 2 mm, obtained by 3D printing by the fused deposition modeling technique, and crosslinked under UV light using Medilux UV 436 HF

(Medilux, Korntal-Münchingen, Germany) lamp (220 V, 60 Hz) for 2 min. Then, coatings with the composition presented in Table 1 were applied to the crosslinked layer and placed under UV light for 4 min. The obtained coatings on PLA plates are presented in Figure 1. In order to measure the thickness, the coatings were scratched/indented in a few regions of the coatings surface. The results are given in Figure 1. The surface morphologies were imaged using a VHX Series Digital Microscope (Keyence, Osaka, Japan). A high-performance camera provided the total image resolution of 4000 pixels (H) \times 3000 pixels (V) with 4 K mode on. The high-resolution HDR function allows observation at magnification from 20 \times down to 2500 \times of low contrasting parts or parts with significant height variation using additional depth composition. The multi-lighting function was used in order to detect the morphology of the coatings presented in Figure 1. The 4 K CMOS Sensor of the VHZ-7000 series (Keyence, Osaka, Japan) allowed to perform 2D and 3D measurements, including measurement of the roughness profile.

Table 1. Coatings composition.

Sample Symbol	PVP (mL)	PEG (mL)	GSH (g)	COL (g)	HA [% w/v]	PEGDA (mL)	Photoinitiator (μ L)
A				-	-		
B	5	5	2	0.04	5	1.8	50
C					15		
D							

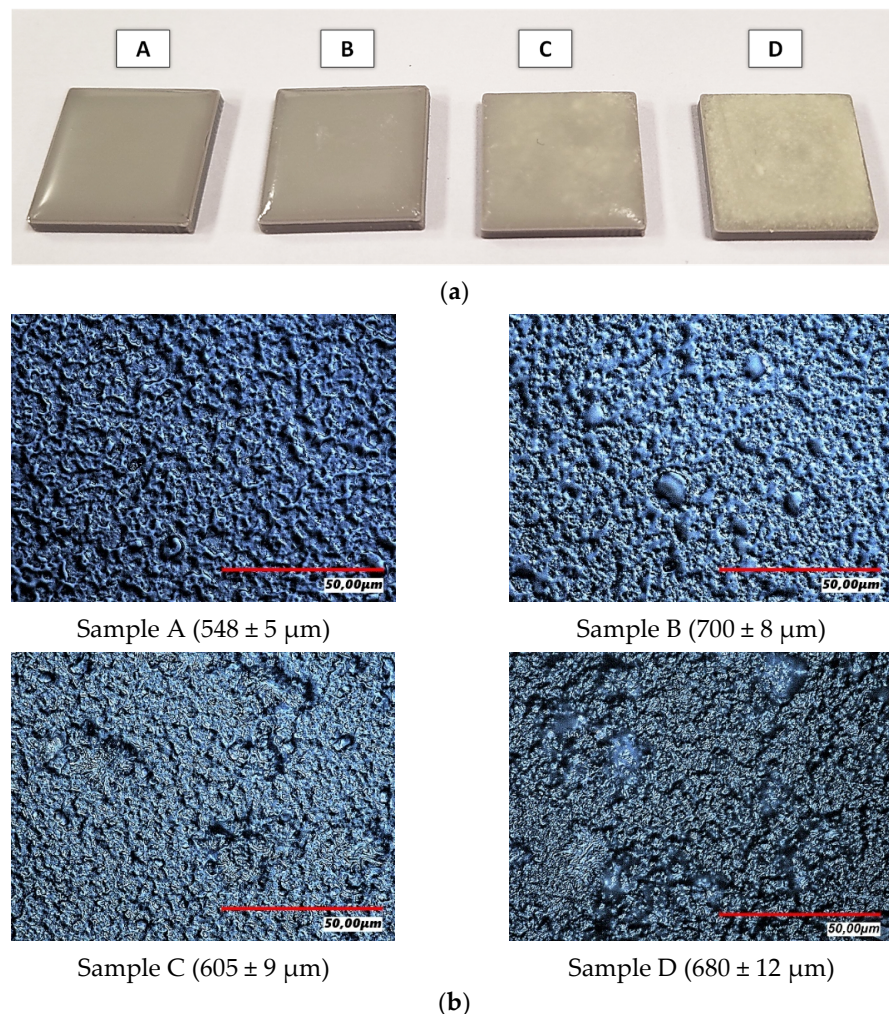


Figure 1. (a) The obtained on PLA plates; (b) high resolution microscope micrographs at magnification 2500 \times , including coatings thicknesses [μ m].

2.3. Fourier-Transform Infrared Spectroscopy Analysis

Fourier transform infrared (FT-IR) spectroscopy was used to identify individual functional groups in pure components (PVP, PEG, COL, GSH, HA) and samples. The analysis was carried out under room conditions using a Nicolet iS5 FT-IR spectrometer equipped with an iD7 ATR attachment (Thermo Scientific, Loughborough, UK) in the range of 4000–400 cm^{-1} (32 scans at 4.0 cm^{-1} resolution).

2.4. Determination of Sorption Capacity

To determine the effect of coatings composition on their swelling kinetic, the prepared samples were incubated in distilled water at 36.6 °C for 7 days. The swelling ability of the coatings immersed in water was calculated in accordance with the following formula:

$$\text{Swelling ability} = \frac{m_1 - m_0}{m_0} \times 100\% \quad (1)$$

where:

m_1 —the weight of immersed sample (g)

m_0 —the initial weight of specimen (g)

The kinetic of coatings swelling was investigated by Voigt-based viscoelastic model Equation (2) [29]. To determine rate parameters and equilibrium swelling, Origin software was used.

$$S_t = S_e [1 - e^{-\frac{t}{\tau}}] \quad (2)$$

where:

S_t —swelling at given time t (%),

S_e —equilibrium swelling (power parameter) (%),

t —time for swelling S_t (min),

τ —the “rate parameter” (min).

2.5. Surface Topography and Roughness

The surface roughness was measured using a stylus line contact profilometer TALY-SURF PGI 830 (Taylor Hobson, San Francisco, CA, USA). Phase Grating Interferometer (PGI) measurement was realized in the relationship between stylus tip movement (input) and response in the gauge head electronics (output) throughout the total measuring range. Stylus arms have a diamond tip with standard coarse tip radius of 2 μm and tip angle of 90°. Surface roughness was determined according to ISO 4287 with stylus acquisition mode from a line distance of 4 mm. The roughness profile, including parameters R_a (roughness), R_q (kurtosis), and R_{sk} (skewness), numerically describe the topography of the measured surfaces. R_a characterizes the departures of the roughness profile from the mean line, and R_q is the rms (root mean square) parameter corresponding to R_a . The skewness (R_{sk}), describing the asymmetry of the profile about the mean line, showed a tendency to be in positive or negative values. The mean value and deviation were determined from at least three repetitions of measurement at different spots on the sample. Ultra TalyMap 5.1. Platinum software (Taylor Hobson, San Francisco, CA, USA) was used for 2D profile and 3D topography analysis and to export the surface images. The composite coatings were additionally evaluated using a Taylor Hobson CCI HD non-contact 3D Optical Profiler.

2.6. Contact Angle and Surface Free Energy

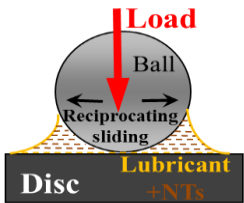
The wettability of samples was measured by the sessile drop method (drop volume—2 μL) followed by image processing using a Drop Shape Analysis (DSA) system 10 Mk2 (Kruss, Germany). In the DSA system, a digital camera measures the parameters of the drop (diameter, height, etc.). In the case of the sessile drop, parameters depend on the angle which the drop forms with the surface. The obtained results are compared with the so-called dimensionless (theoretical) profiles, which are solutions of the Laplace–Young equation [30].

The contact angle was determined for a polar solvent, which was ultra-high quality (UHQ) water of resistivity 18 M Ω /cm, and non-polar diodomethane. Surface free energy was calculated according to Owens–Wendt–Rebel–Keeble approach [31]. The averaged contact angle values and the surface free energy of each tested sample was determined from at least three repetitions of measurement at different spots on the sample. The standard deviation of the surface free energy was determined according to the error propagation method.

2.7. Nanotribometer

For friction force measurements of coatings, the NTR2 Nanotribometer (CSM Instruments SA, Freiburg, Germany) was used. It can conduct both linear reciprocating and rotating modes. The device enables to control the following test parameters: speed, load, distance, time, and frequency. The motion resistance is determined during the test by measuring the deflection of the elastic arm with the ball or pin sample. The measurements were conducted for 1 h at 25 °C under a normal load of 500 mN and at an average speed of 1 cm/s (3.18 Hz). The test conditions are given in Table 2.

Table 2. Detailed parameters used for friction force measurements of coatings.

Tribological Test Set-Up	
Contact conditions	Point contact at reciprocating sliding
Track length	1 mm
Speed	average 1 cm/s (3.18 Hz)
Normal Load	500 mN
Mean contact pressure	50 MPa
Temperature	25 °C
Test duration	1 h
Measured parameters	Coefficient of friction vs. time and wear volume

2.8. Hardness Measurement of Coatings

To determine the effect of the ceramic phase on the hardness of the coatings, Shore A hardness was measured using a Zwick 3130, ZwickRoell GmbH & Co. KG, Ulm, Germany. The measurement was performed with a load of 10 Newtons.

3. Results and Discussion

3.1. Fourier-Transform Infrared Spectroscopy Analysis

The FTIR analysis performed in this study was used as a qualitative investigation to confirm the identity of the pure components and the developed coatings.

Figure 2 shows FTIR absorbance spectra of pure components PVP, PEG, COL, GSH, HA, and coating compositions. The characteristic stretching and bending vibration of the functional groups are exhibited on the FTIR spectra.

Analyzing the spectra of the composites coatings clearly shows the peaks coming from the base polymers, which are PVP and PEG. This is particularly evident in the spectra of all composite coatings, where the peak at 1660 cm⁻¹ is attributed to the C=O bonds originating from PVP [32]. At 1270 cm⁻¹ and 2875 cm⁻¹, the CH₂ group was observed in polymers that are present in the obtained coatings [33].

The glutathione spectrum identified a -CN group at 1080 cm⁻¹, a -CH group at 1310 cm⁻¹, and a -COO group at 1624 cm⁻¹ [34]. The spectrum of samples B, C, and D shows peaks of amide I at 1740 cm⁻¹, amide II at 1630 cm⁻¹, and a set of three weaker bands that represent amide III vibration modes centered at 1230 cm⁻¹, originating from

collagen [35]. It is worth noting that these peaks overlap with the peaks from the polymers. In samples C and D, spectral analysis revealed the presence of phosphate groups as evidenced by distinct bands in the 560–1023 cm^{-1} range. The peaks at 560 cm^{-1} and 575 cm^{-1} originate from triple degenerate O-P-O bending modes in PO_4^{3-} . The peak occurring at 1023 cm^{-1} is associated with asymmetric P-O stretching vibrations [36].

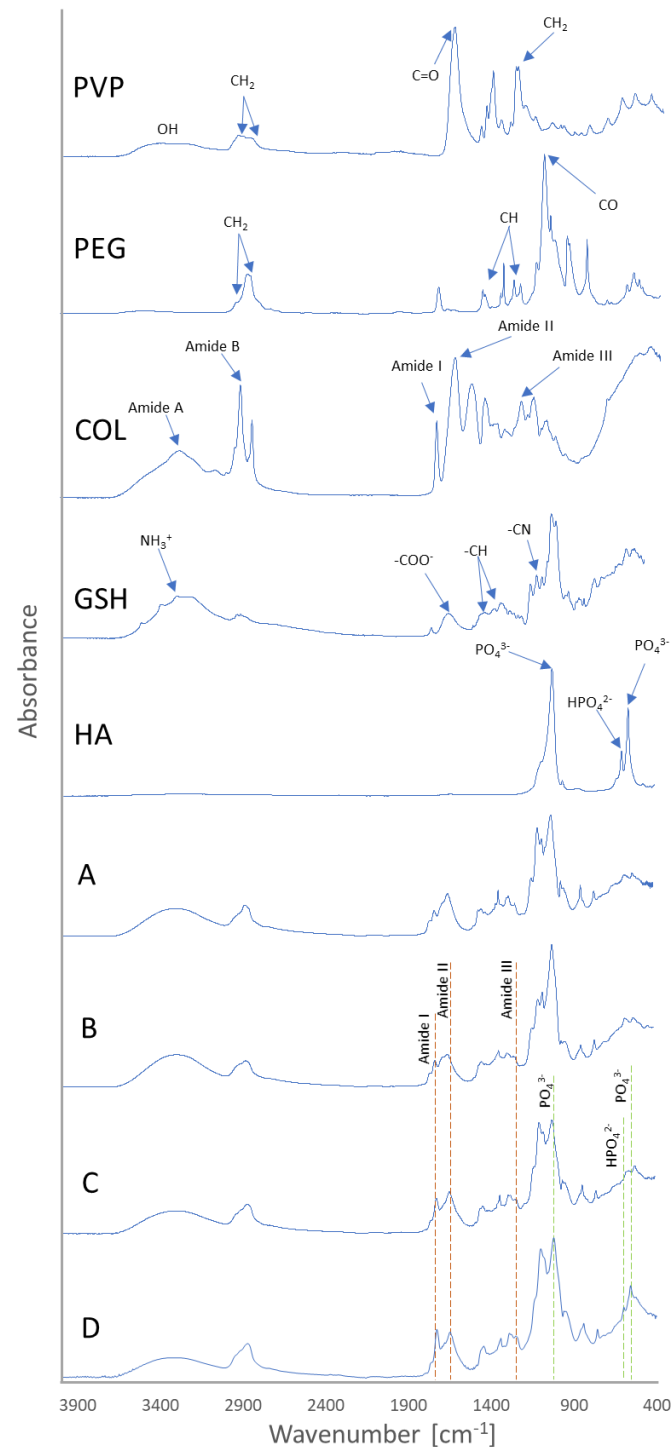


Figure 2. FTIR spectra of PVP, PEG, COL, GSH, HA and coatings.

3.2. Determination of Sorption Capacity

In Figure 3, the swelling kinetics of the tested coated materials immersed in distilled water for 7 days is presented. Equilibrium swelling and rate parameters (τ) are shown in

Table 3. The equilibrium swelling of coatings was in the range of 82.5 ± 2.8 – $118.8 \pm 5.1\%$, and the lowest swelling capacity was recorded for sample D containing 15% *w/v* of HA. It can be observed that the equilibrium swelling of materials is strongly dependent on their composition. The addition of ceramic at variable contents leads to a decrease in material equilibrium swelling in comparison with the polymeric coating, as shown in Table 3. Moreover, it is shown that composite coatings (samples C and D) are also characterized with greater rate parameters (τ) as compared to polymeric coatings (samples A and B). Thus, it can be concluded that the addition of ceramic leads to the decreased swelling ability of materials and slower liquid medium absorption by composite coatings [15].

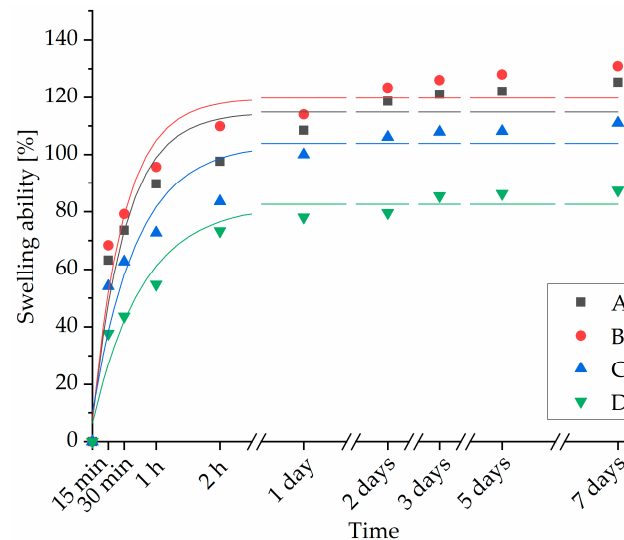


Figure 3. Swelling kinetics of coatings in distilled water. Solid lines indicate fittings for the swelling ability of individual samples.

Table 3. Rate parameter (τ) and equilibrium swelling (S_e) of tested samples.

Sample	S_e [%]	τ
A	115.8 ± 5.0	30.41 ± 8.1
B	118.8 ± 5.1	29.7 ± 8.0
C	103.8 ± 4.5	41.14 ± 10.9
D	82.5 ± 2.8	47.3 ± 9.2

3.3. Surface Topography and Roughness

The composite coatings PVP/PEG/GSH were evaluated using a Taylor Hobson CCI HD non-contact 3D Optical Profiler. Results of the analysis of the surface topography of tested samples are presented in Figure 4. By analyzing the results, the effect of HAP addition on the surface topography can be seen. As the proportion of ceramic phase increases, the surface becomes less regular, rougher, and wavier. Results of the analysis of the surface topography of tested samples are presented in Figure 4.

Surface roughness was measured according to ISO 4287 with contact stylus acquisition mode in a line distance of 4 mm. Roughness profile and acquired roughness parameters are given in Figure 5. By comparing all the composite coatings, sample A (PVP/PEG/GSH) shows the lowest surface roughness value, R_a (1.41 ± 0.38), which indicates that it is the smoothest surface, as visible in topography image in Figure 4a. In contrast, sample D (PVP/PEG/GSH/collagen and HA 15 wt.%) shows the highest R_a (6.10 ± 0.87) value, followed by sample C (PVP/PEG/GSH/collagen and HA 5 wt.%) with an R_a value (3.76 ± 0.61). According to these results, it can be concluded that the addition of HA strongly increases the surface roughness due to the presence of grains of HA on the surface (red wide dots) visible on Figure 4c,d. The addition of collagen in comparison to the basic

matrix sample A resulted in the formation of small sharp peaks on the surface presented in surface topography Figure 4b. However, the roughness value Ra is increased marginally. Meanwhile, the presence of HA in 15% wt.% content (sample D) increased Ra and Rq values strongly when compared to the original polymer matrix, sample A (visible in Figure 5a,d). In general root mean square follows Ra values, increasing from sample A to D, following the amount of HA in the coating. Only skewness is unsimilar in describing the asymmetry, which is positive from samples A, B, and D consisting predominately of peak asperities visible in Figure 5a,b,d. Skewness for sample C is negative, representing surfaces that consist primarily of valleys, which can be clearly observed in Figure 5c. Rsk is an excellent parameter for measuring surfaces that are expected to have peaks or valleys. However, if a surface has been largely planarized such that a few peaks or valleys remain, then Rsk returns to nearly zero, which is the case for samples A, C, and D.

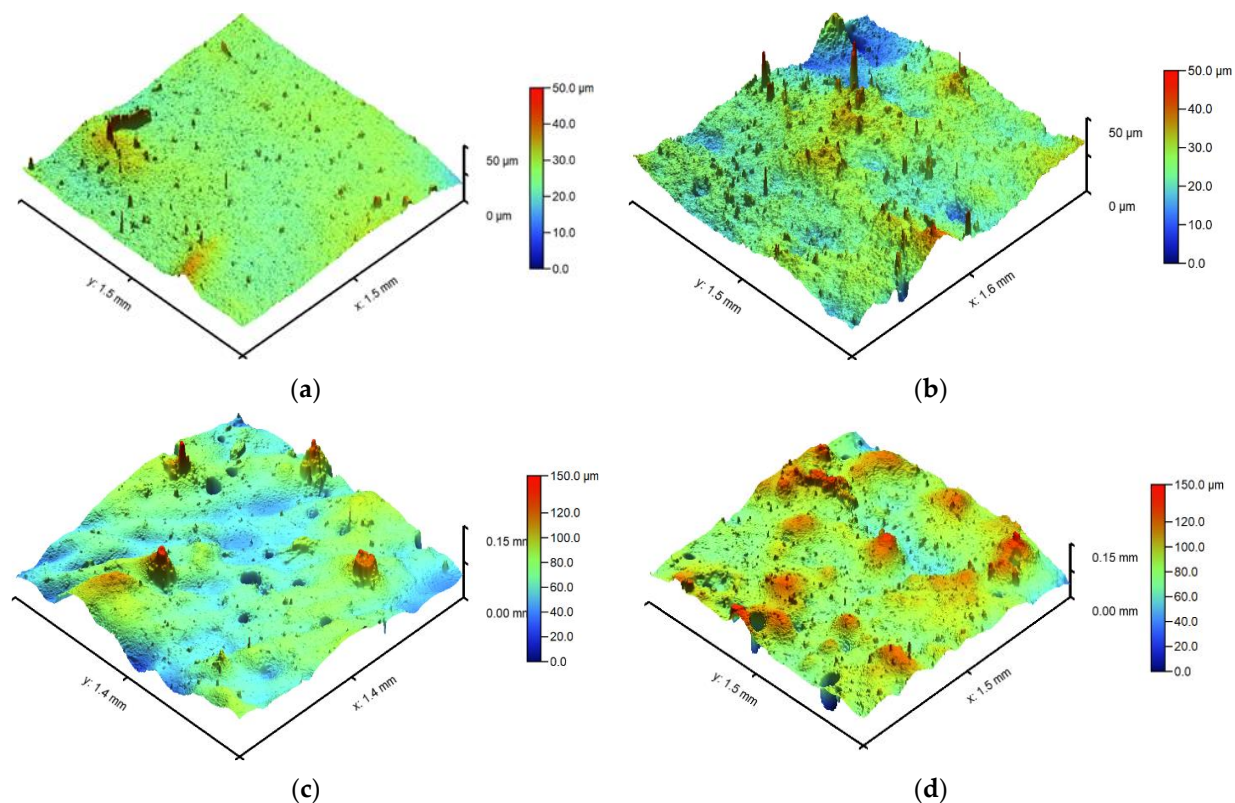


Figure 4. Surface topography of composite coatings for (a) sample A; (b) sample B; (c) sample C; (d) sample D.

3.4. Contact Angle and Surface Free Energy

In Table 4, the water contact angle and polar surface free energy calculated for it (Owens–Wendt–Kaelble approach) are listed, as well as the diiodomethane contact angle and dispersive surface free energy calculated for it. Total surface free energy is the sum of both components.

Sample A, the reference coating containing only PVP/PEG/GSH, has similar wettability for the polar component (water) to sample B, additionally containing collagen, resulting in a similar total free surface energy for both samples. This outcome can be also explained by similar roughness parameters for both samples. The presence of HA in coatings C and D decreased contact angles for polar and non-polar fluids and increased the total free surface energy when compared to samples A and B. The highest free surface energy can be noted for coating C, composed of PVP/PEG/GSH/collagen and HA 5 wt.%, which can be correlated with negative Rsk skewness for the surface that consists primarily of valleys (Figure 5c).

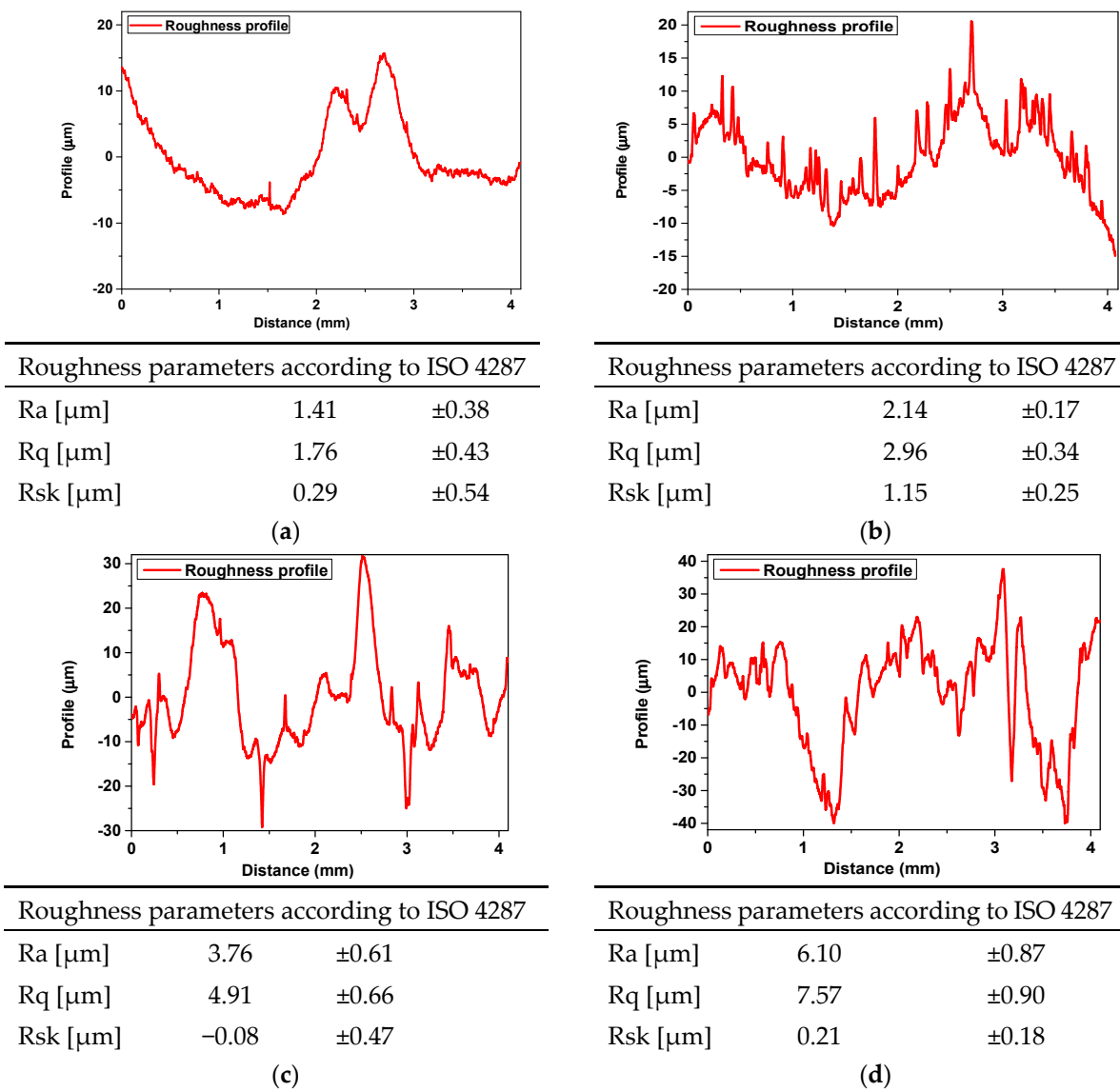


Figure 5. Surface roughness profile and parameters of a composite coatings (a) A—PVP/PEG/GSH; (b) B—PVP/PEG/GSH/COL; (c) C—PVP/PEG/GSH/COL and HAP 5 wt.%; (d) D—PVP/PEG.GSH/COL and HAP 15 wt.%.

Table 4. Contact angles and surface free energies for samples A—D.

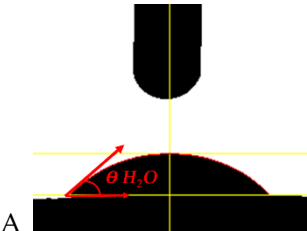
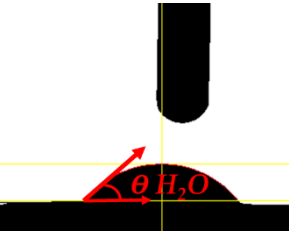
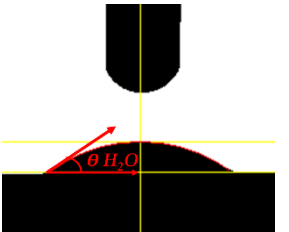
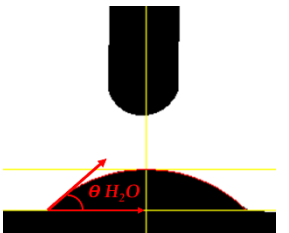
Sample Symbol and H ₂ O Drop Shape	θ_{H_2O} [°]—Contact Angle for Polar Fluid	θ_{DJD} [°]—Contact Angle for Non-Polar Fluid	δ_s^P [mJ/m ²] Surface Energy for Water	δ_s^D [mJ/m ²] Surface Energy for Djd	δ_s [mJ/m ²] Free Surface Energy
	50.3 ± 1.3	35.0 ± 1.6	24.80	25.17	49.97

Table 4. Cont.

Sample Symbol and H ₂ O Drop Shape	θ_{H_2O} [°]—Contact Angle for Polar Fluid	θ_{DJD} [°]—Contact Angle for Non-Polar Fluid	δ_s^P [mJ/m ²] Surface Energy for Water	δ_s^D [mJ/m ²] Surface Energy for DjD	δ_s [mJ/m ²] Free Surface Energy
B 	53.7 ± 2.0	26.27 ± 0.4	18.64	31.04	49.68
C 	40.1 ± 1.9	28.4 ± 1.0	32.30	24.74	57.04
D 	46.0 ± 1.9	27.1 ± 1.2	26.15	27.42	53.57

3.5. Nanotribometer

The coefficient of friction (CoF) of the coatings based on PVP/PEG and glutathione was investigated based on a reciprocating sliding test with a nanotribometer. The tribological performance of tested coatings was evaluated with an Al₂O₃ ball most-representative material configuration. Preliminarily, parameters were adjusted to follow ASTM standard. Unfortunately, it turned out that the conditions were too harsh. Further, the conditions were adopted for the PVP/PEG coatings and set as presented in Table 2: load of 500 mN and speed of 1 cm/s for 1 h at room temperature. The averaged friction scans as a function of time are presented in Figure 6a. The error bars visible on the friction curves represent the reproducibility of three repetitional tests. Directly after the frictional test, the wear tracks analysis on the tested samples was performed using a 3D Optical Profiler Interferometric System. The volume analysis method estimates the volume between the worn surface and a reference plane. The reference plane was set as the average height of the unworn area outside the wear track. The wear volume was calculated for the whole wear track, and only the area under the reference plane was considered.

The highest friction visible in Figure 6a was noted for reference sample A, which is related to the insufficient mechanical strength of this coating. When in contact with PBS fluid especially, the coating become too soft to perform the test. Thus, it was carried out in dry contact conditions. Moreover, as can be observed in Figure 6a, the black curve representing coating A is most unstable and oscillating, due which the error bars are also higher. As expected, high friction values lead to high wear volume, as presented in the columnar graph at Figure 6b, which is also related to poor mechanical strength. Sample B which was additionally composed of collagen in comparison to sample A presents a very low coefficient of friction, high frictional scan reproducibility, and low wear rate. The collagen component clearly has a beneficial effect on the tribological properties of the PVP/PEG coatings, also affecting an improvement of the mechanical strength. The

addition of HA ceramic at increasing contents led to a slow increase of CoF μ and wear rate. The addition of HA ceramic phase in 5% to sample C is represented by the blue frictional scan and blue column on the wear rate graph (Figure 6a,b). As presented, the CoF and wear volume are still satisfactory low. The situation changes when too much HA phase is added to the polymeric PVA/PVP compound, as is the case for sample D represented by the CoF pink curve and wear column bar. Although the COF is not the highest (Figure 6a) the wear increases evidently (Figure 6b). This behaviour can be explained by the crushing and crumbling of the small particles of HA from the very rough PVA/PVP compound coating, causing these particles to have a strong abrasive effect of on the sample D surface. This explains why the friction is not very high, as the particles by rolling in contact reduce friction, although causing surface damage.

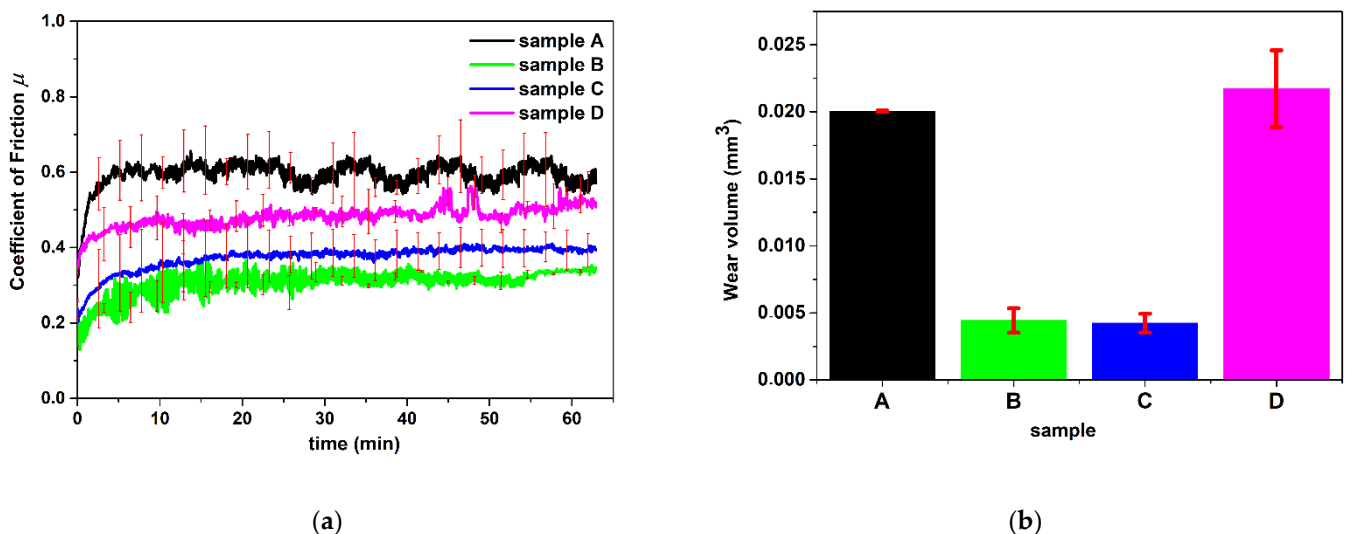


Figure 6. Nanotribometer tests result represented with friction curves including error bars distribution over the curve (a) and wear volume bar graphs measured with 3D Optical Profiler Interferometric System (b).

The surfaces of the coatings based on PVP/PEG, glutathione, collagen, and HA after the reciprocating sliding test with a nanotribometer were thoroughly investigated with optical and interferometric microscopes, the results of which are presented in Figure 7a–d. The length, width, and depth of the wear scar was measured, as well as the roughness parameters inside the track. The surface height parameters measured for area (kurtosis S_q , skewness S_{sk} , and roughness S_a) quantitatively describe the damaged wear track. As can be observed, the rough wear zone for samples A and D (Figure 7a,d) correlates with the high wear volume in Figure 6b. The lowest wear volume and at the same time minimal damage and lowest CoF can be observed for sample B, which contains collagen and 0% HA, and for sample C, which contains collagen and 5% HA.

3.6. Hardness Measurement of Coatings

Figure 8 presents the results obtained for the Shore A hardness measurements for the obtained composite coatings. In the case of coatings without the contribution of the ceramic phase, i.e., A and B, relatively similar results oscillating around the value of 85 were obtained. However, the influence of HA on the hardness can be seen, as the value clearly increases with an increase in the contribution of HA to the materials. However, it is important to note that the hardness measurements were also influenced by PLA plates. Considering the thickness of the applied ceramic–polymer coating on the PLA, it is possible that the PLA plate had a significant impact on the measurement result.

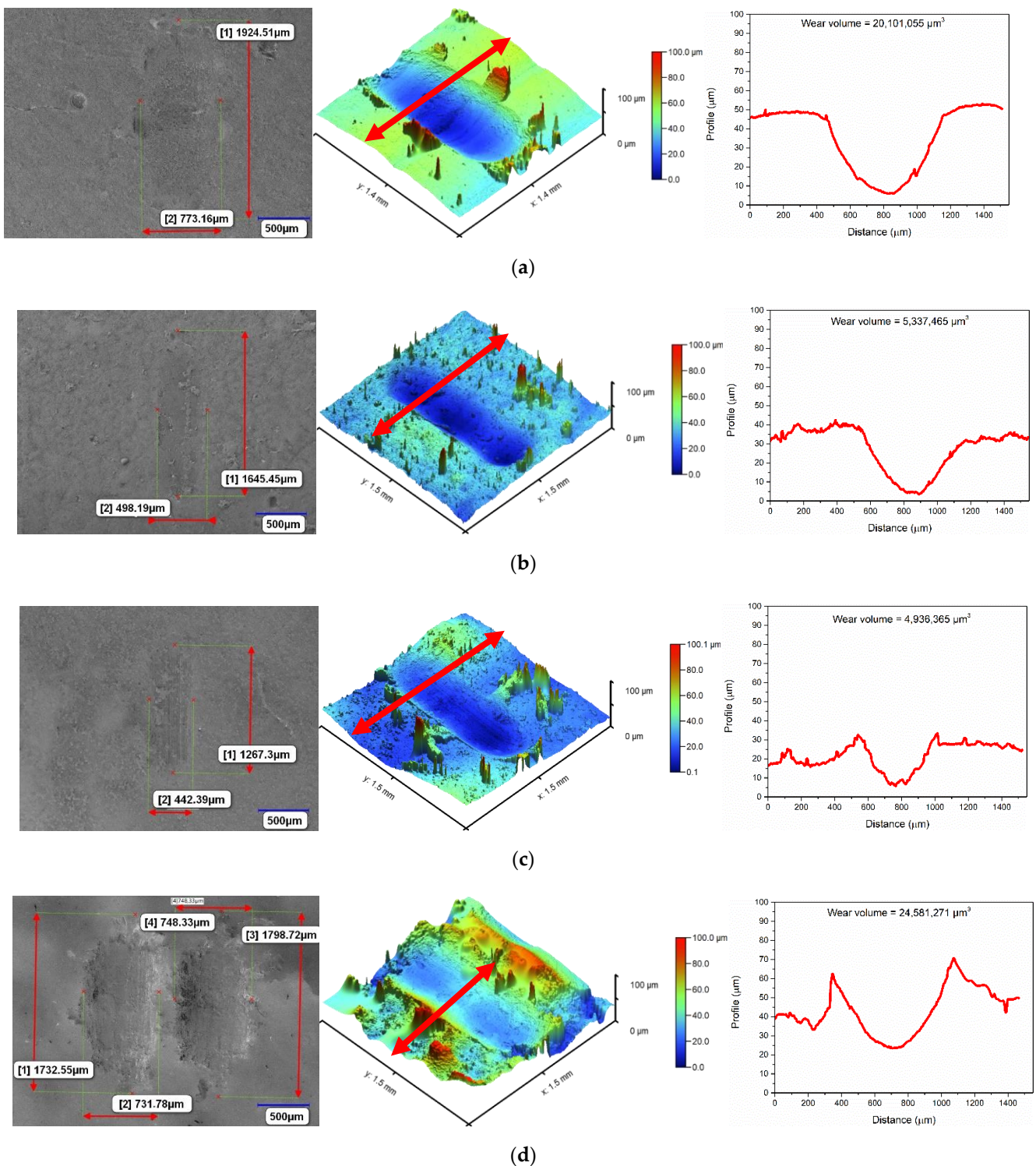


Figure 7. Wear tracks topography after nanotribometer tests: optical and interferometric micrographs including roughness parameters within the wear track for samples A–D (a–d). Cross section of the surface profile is marked on the interferometric image and presented as a graph. (a) Sample A, roughness inside the wear score: $S_a = 7.89 \mu\text{m}$, $S_q = 9.66 \mu\text{m}$, $S_{sk} = 0.2 \mu\text{m}$. (b) Sample B, roughness inside the wear score: $S_a = 1.58 \mu\text{m}$, $S_q = 1.89 \mu\text{m}$, $S_{sk} = 0.4 \mu\text{m}$. (c) Sample C, roughness inside the wear score: $S_a = 3.59 \mu\text{m}$, $S_q = 4.42 \mu\text{m}$, $S_{sk} = 0.36 \mu\text{m}$. (d) Sample D, roughness inside the wear score: $S_a = 6.14 \mu\text{m}$, $S_q = 7.56 \mu\text{m}$, $S_{sk} = 0.46 \mu\text{m}$.

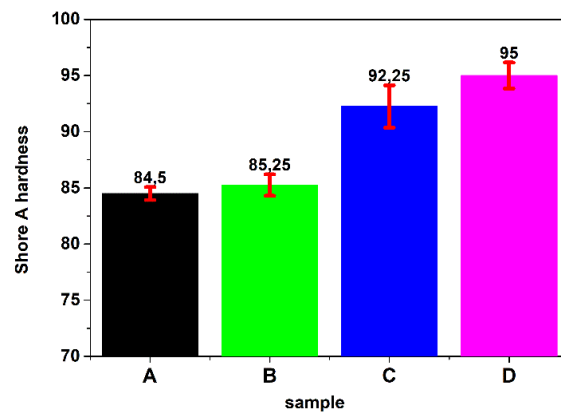


Figure 8. Hardness measurement of coatings by the shore method A.

However, the results obtained are consistent with literature reports on composites with ceramics [37,38].

4. Conclusions

We can assume that the preparation method of PVP/PEG/GSH/COL/HA coatings on PLA plates was successful. The developed technology as well as the choice of crosslinking agent and photoinitiator allowed to perform the photocrosslinking process under UV light without any by-products. Moreover, the coatings were fully crosslinked, and the ceramics did not crumble. Good integrity was also achieved, as the coating was fully continuous and uniformly crosslinked, with no significant irregularities or holes. Last but not least, high adhesion was obtained, with the coating fully and permanently adhered to the PLA wafer, and good adhesion was observed for both wet and dried coatings. Moreover, the coatings exhibited good mechanical strength and a well-developed surface morphology and topography. The nanotribometric reciprocating sliding test method showed excellent tribological properties of the composites coating containing collagen and a small amount (5%) of HA ceramic phase. Meanwhile, the ceramic phase in too high a content (15%) decreased the swelling ability of composites and slowed liquid medium absorption, additionally causing surface roughening. In consequence, during the reciprocating sliding test, small and hard particles of HA from the very rough composite are crushed, having a strong abrasive effect on the sample surface and loosening tribological properties. It can be concluded that sample C composed of PVP/PEG/GSH/COL/HA(5%) exhibits high biological value for its osteoconductivity, strong mechanical and tribological properties, highest free surface energy, as well as porosity and accepted roughness to be implemented as safe materials for bone regeneration. No such materials with the same or similar composition designed for bone tissue regeneration are available in the literature so far. Therefore, given the satisfactory results, further studies, especially physicochemical and biological, are needed to confirm the biosafety and the absence of cytotoxicity.

Author Contributions: Conceptualization, A.M.T. and D.S.; data curation, A.M.T., D.S. and M.D.; formal analysis, D.S. and A.S.-K.; funding acquisition, A.S.-K.; investigation, A.M.T.; methodology, A.M.T., D.S. and K.P.; project administration, A.S.-K.; software, W.F. and K.P.; supervision, A.M.T. and A.S.-K.; validation, A.M.T., D.S., W.F. and M.D.; visualization, D.S., W.F. and K.P.; writing—original draft, A.M.T. and D.S.; writing—review and editing, W.F. All authors have read and agreed to the published version of the manuscript.

Funding: This research was funded by Foundation for Polish Science, grant number POIR.04.04.00-00-16D7/18.

Institutional Review Board Statement: Not applicable.

Informed Consent Statement: Not applicable.

Data Availability Statement: The data that support the findings of this study are contained within the article.

Acknowledgments: The “Multifunctional biologically active composites for applications in bone regenerative medicine” project is carried out within the TEAM-NET program of the Foundation for Polish Science financed by the European Union under the European Regional Development Fund. The authors gratefully acknowledge financial support.

Conflicts of Interest: The authors declare no conflict of interest.

References

1. Djošić, M.; Janković, A.; Mišković-Stanković, V. Electrophoretic Deposition of Biocompatible and Bioactive Hydroxyapatite-Based Coatings on Titanium. *Materials* **2021**, *14*, 5391. [[CrossRef](#)]
2. Chevallier, P.; Turgeon, S.; Sarra-Bournet, C.; Turcotte, R.; Laroche, G. Characterization of Multilayer Anti-Fog Coatings. *ACS Appl. Mater. Interfaces* **2011**, *3*, 750–758. [[CrossRef](#)] [[PubMed](#)]
3. Soon, G.; Pingguan-Murphy, B.; Lai, K.W.; Akbar, S.A. Review of Zirconia-Based Bioceramic: Surface Modification and Cellular Response. *Ceram. Int.* **2016**, *42*, 12543–12555. [[CrossRef](#)]
4. Eliaz, N.; Metoki, N. Calcium Phosphate Bioceramics: A Review of Their History, Structure, Properties, Coating Technologies and Biomedical Applications. *Materials* **2017**, *10*, 334. [[CrossRef](#)] [[PubMed](#)]
5. Spraying, D. Creation of Bioceramic Coatings on the Surface of Ti–6Al–4V Detonation Spraying. *Coatings* **2021**, *11*, 1433.
6. Li, J.; Jansen, J.A.; Walboomers, X.F.; van den Beucken, J.J. Mechanical Aspects of Dental Implants and Osseointegration: A Narrative Review. *J. Mech. Behav. Biomed. Mater.* **2020**, *103*, 103574. [[CrossRef](#)]
7. Kaneko, S.; Yamamoto, Y.; Wada, K.; Kumagai, G.; Harada, Y.; Yamauchi, R.; Ishibashi, Y. Ultraviolet Irradiation Improves the Hydrophilicity and Osteo-Conduction of Hydroxyapatite. *J. Orthop. Surg. Res.* **2020**, *15*, 425. [[CrossRef](#)]
8. Bai, L.; Liu, Y.; Du, Z.; Weng, Z.; Yao, W.; Zhang, X.; Huang, X.; Yao, X.; Crawford, R.; Hang, R.; et al. Differential Effect of Hydroxyapatite Nano-Particle versus Nano-Rod Decorated Titanium Micro-Surface on Osseointegration. *Acta Biomater.* **2018**, *76*, 344–358. [[CrossRef](#)]
9. Xia, L.; Xie, Y.; Fang, B.; Wang, X.; Lin, K. In Situ Modulation of Crystallinity and Nano-Structures to Enhance the Stability and Osseointegration of Hydroxyapatite Coatings on Ti-6Al-4V Implants. *Chem. Eng. J.* **2018**, *347*, 711–720. [[CrossRef](#)]
10. Um, S.H.; Chung, Y.W.; Seo, Y.; Seo, H.; Ok, M.R.; Kim, Y.C.; Han, H.S.; Chung, J.J.; Edwards, J.R.; Jeon, H. Robust Hydroxyapatite Coating by Laser-Induced Hydrothermal Synthesis. *Adv. Funct. Mater.* **2020**, *30*, 2005233. [[CrossRef](#)]
11. Beig, B.; Liaqat, U.; Niazi, M.F.K.; Douna, I.; Zahoor, M.; Niazi, M.B.K. Current Challenges and Innovative Developments in Hydroxyapatite-Based Coatings on Metallic Materials for Bone Implantation: A Review. *Coatings* **2020**, *10*, 1249. [[CrossRef](#)]
12. Ullah, I.; Siddiqui, M.A.; Liu, H.; Kolawole, S.K.; Zhang, J.; Zhang, S.; Ren, L.; Yang, K. Mechanical, Biological, and Antibacterial Characteristics of Plasma-Sprayed (Sr,Zn) Substituted Hydroxyapatite Coating. *ACS Biomater. Sci. Eng.* **2020**, *6*, 1355–1366. [[CrossRef](#)] [[PubMed](#)]
13. Chen, Y.; Ren, J.; Liu, W.; Zhao, D. Enhanced Scratch Performance of Plasma Sprayed Hydroxyapatite Composite Coatings Reinforced with BN Nanoplatelets. *Coatings* **2020**, *10*, 652. [[CrossRef](#)]
14. Zhao, H.; Liao, J.; Wu, F.; Shi, J. Mechanical Strength Improvement of Chitosan/Hydroxyapatite Scaffolds by Coating and Cross-Linking. *J. Mech. Behav. Biomed. Mater.* **2021**, *114*, 104169. [[CrossRef](#)] [[PubMed](#)]
15. Jung, H.G.; Lee, D.; Lee, S.W.; Kim, I.; Kim, Y.; Jang, J.W.; Lee, J.H.; Lee, G.; Yoon, D.S. Nanoindentation for Monitoring the Time-Variant Mechanical Strength of Drug-Loaded Collagen Hydrogel Regulated by Hydroxyapatite Nanoparticles. *ACS Omega* **2021**, *6*, 9269–9278. [[CrossRef](#)] [[PubMed](#)]
16. Banoriya, D.; Purohit, R.; Dwivedi, R.K. Advanced Application of Polymer Based Biomaterials. *Mater. Today Proc.* **2017**, *4*, 3534–3541. [[CrossRef](#)]
17. Grant, J.J.; Pillai, S.C.; Perova, T.S.; Hehir, S.; Hinder, S.J.; McAfee, M.; Breen, A. Electrospun Fibres of Chitosan/PVP for the Effective Chemotherapeutic Drug Delivery of 5-Fluorouracil. *Chemosensors* **2021**, *9*, 70. [[CrossRef](#)]
18. Ozkan, G.; Franco, P.; Capanoglu, E.; De Marco, I. PVP/Flavonoid Coprecipitation by Supercritical Antisolvent Process. *Chem. Eng. Process.—Process Intensif.* **2019**, *146*, 107689. [[CrossRef](#)]
19. López-Calderón, H.D.; Avilés-Arnaut, H.; Galán Wong, L.J.; Almaguer-Cantú, V.; Laguna-Camacho, J.R.; Calderón-Ramón, C.; Escalante-Martínez, J.E.; Arévalo-Niño, K. Electrospun Polyvinylpyrrolidone-Gelatin and Cellulose Acetate Bi-Layer Scaffold Loaded with Gentamicin as Possible Wound Dressing. *Polymers* **2020**, *12*, 2311. [[CrossRef](#)]
20. Voronova, M.; Rubleva, N.; Kochkina, N.; Afineevskii, A.; Zakharov, A.; Surov, O. Preparation and Characterization of Polyvinylpyrrolidone/Cellulose Nanocrystals Composites. *Nanomaterials* **2018**, *8*, 1011. [[CrossRef](#)]
21. Bakaic, E.; Smeets, N.M.B.; Hoare, T. Injectable Hydrogels Based on Poly(Ethylene Glycol) and Derivatives as Functional Biomaterials. *RSC Adv.* **2015**, *5*, 35469–35486. [[CrossRef](#)]
22. Knop, K.; Hoogenboom, R.; Fischer, D.; Schubert, U.S. Poly(Ethylene Glycol) in Drug Delivery: Pros and Cons as Well as Potential Alternatives. *Angew. Chem.—Int. Ed.* **2010**, *49*, 6288–6308. [[CrossRef](#)] [[PubMed](#)]
23. Thi, T.T.H.; Pilkington, E.H.; Nguyen, D.H.; Lee, J.S.; Park, K.D.; Truong, N.P. The Importance of Poly(Ethylene Glycol) Alternatives for Overcoming PEG Immunogenicity in Drug Delivery and Bioconjugation. *Polymers* **2020**, *12*, 298. [[CrossRef](#)]

24. Chakravarty, J.; Rabbi, M.F.; Chalivendra, V.; Ferreira, T.; Brigham, C.J. Mechanical and Biological Properties of Chitin/Poly lactide (PLA)/Hydroxyapatite (HAP) Composites Cast Using Ionic Liquid Solutions. *Int. J. Biol. Macromol.* **2020**, *151*, 1213–1223. [[CrossRef](#)] [[PubMed](#)]
25. Serra, T.; Mateos-Timoneda, M.A.; Planell, J.A.; Navarro, M. 3D Printed PLA-Based Scaffolds: A Versatile Tool in Regenerative Medicine. *Organogenesis* **2013**, *9*, 239–244. [[CrossRef](#)]
26. Munirah, S.; Kim, S.H.; Ruszymah, B.H.I.; Khang, G. The Use of Fibrin and Poly(Lactic-Co-Glycolic Acid) Hybrid Scaffold for Articular Cartilage Tissue Engineering: An in Vivo Analysis. *Eur. Cells Mater.* **2008**, *15*, 41–52. [[CrossRef](#)]
27. Gregor, A.; Filová, E.; Novák, M.; Kronek, J.; Chlup, H.; Buzgo, M.; Blahnová, V.; Lukášová, V.; Bartoš, M.; Nečas, A.; et al. Designing of PLA Scaffolds for Bone Tissue Replacement Fabricated by Ordinary Commercial 3D Printer. *J. Biol. Eng.* **2017**, *11*, 31. [[CrossRef](#)]
28. Słota, D.; Florkiewicz, W.; Piętak, K.; Szwed, A.; Włodarczyk, M.; Siwińska, M.; Rudnicka, K.; Sobczak-Kupiec, A. Preparation, Characterization, and Biocompatibility Assessment of Polymer-Ceramic Composites Loaded with *Salvia officinalis* Extract. *Materials* **2021**, *14*, 6000. [[CrossRef](#)]
29. Kabiri, K.; Omidian, H.; Hashemi, S.A.; Zohuriaan-Mehr, M.J. Synthesis of Fast-Swelling Superabsorbent Hydrogels: Effect of Crosslinker Type and Concentration on Porosity and Absorption Rate. *Eur. Polym. J.* **2003**, *39*, 1341–1348. [[CrossRef](#)]
30. Marmur, A. Thermodynamic Aspects of Contact Angle Hysteresis. *Adv. Colloid Interface Sci.* **1994**, *50*, 121–141. [[CrossRef](#)]
31. Owens, D.K.; Wendt, R.C. Estimation of the Surface Free Energy of Polymers. *J. Appl. Polym. Sci.* **1969**, *13*, 1741–1747. [[CrossRef](#)]
32. Abdelghany, A.M.; Mekhail, M.S.; Abdelrazek, E.M.; Aboud, M.M. Combined DFT/FTIR structural studies of monodispersed PVP/Gold and silver nano particles. *J. Alloys Compd.* **2015**, *646*, 326–332. [[CrossRef](#)]
33. Deygen, I.M.; Kudryashova, E.V. New Versatile Approach for Analysis of PEG Content in Conjugates and Complexes with Biomacromolecules Based on FTIR Spectroscopy. *Colloids Surf. B Biointerfaces* **2016**, *141*, 36–43. [[CrossRef](#)] [[PubMed](#)]
34. Negishi, Y.; Nobusada, K.; Tsukuda, T. Glutathione-Protected Gold Clusters Revisited: Bridging the Gap between Gold(I)-Thiolate Complexes and Thiolate-Protected Gold Nanocrystals. *J. Am. Chem. Soc.* **2005**, *127*, 5261–5270. [[CrossRef](#)]
35. De Campos Vidal, B.; Mello, M.L.S. Collagen Type I Amide I Band Infrared Spectroscopy. *Micron* **2011**, *42*, 283–289. [[CrossRef](#)]
36. Rehman, I.; Bonfield, W. Characterization of Hydroxyapatite and Carbonated Apatite by Photo Acoustic FTIR Spectroscopy. *J. Mater. Sci. Mater. Med.* **1997**, *8*, 1–4. [[CrossRef](#)]
37. Nihmath, A.; Ramesan, M.T. Development of Hydroxyapatite Nanoparticles Reinforced Chlorinated Acrylonitrile Butadiene Rubber/Chlorinated Ethylene Propylene Diene Monomer Rubber Blends. *J. Appl. Polym. Sci.* **2021**, *138*, 50189. [[CrossRef](#)]
38. Verma, N.; Zafar, S.; Talha, M. Influence of Nano-Hydroxyapatite on Mechanical Behavior of Microwave Processed Polycaprolactone Composite Foams. *Mater. Res. Express* **2019**, *6*, 085336. [[CrossRef](#)]